

Selective particle capture by asynchronously beating cilia

Yang Ding and Eva Kanso

Citation: *Physics of Fluids* **27**, 121902 (2015); doi: 10.1063/1.4938558

View online: <http://dx.doi.org/10.1063/1.4938558>

View Table of Contents: <http://scitation.aip.org/content/aip/journal/pof2/27/12?ver=pdfcov>

Published by the [AIP Publishing](#)

Articles you may be interested in

[Bacterial response to different surface chemistries fabricated by plasma polymerization on electrospun nanofibers](#)

Biointerphases **10**, 04A301 (2015); 10.1116/1.4927218

[Impact of tortuous flow on bacteria streamer development in microfluidic system during filtration](#)

Biomicrofluidics **8**, 014105 (2014); 10.1063/1.4863724

[The effect of nanofiber based filter morphology on bacteria deactivation during water filtration](#)

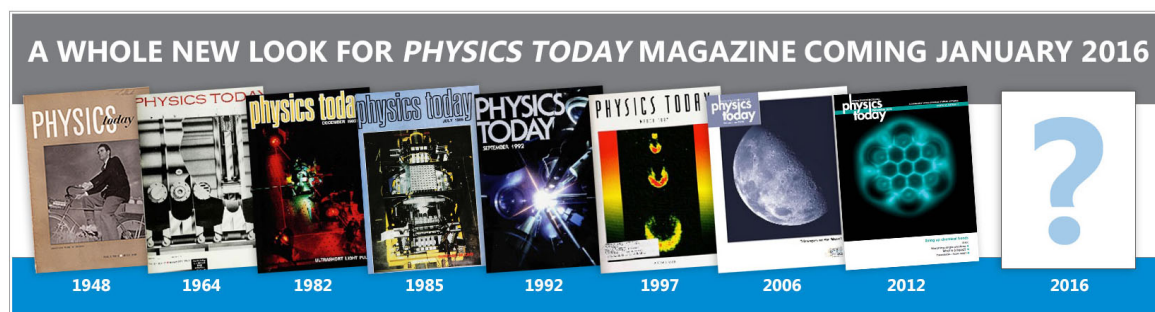
AIP Conf. Proc. **1526**, 316 (2013); 10.1063/1.4802626

[Continuous field-flow separation of particle populations in a dielectrophoretic chip with three dimensional electrodes](#)

Appl. Phys. Lett. **90**, 234104 (2007); 10.1063/1.2747187

[Probing microplatform for the study of biological adhesion forces](#)

Rev. Sci. Instrum. **74**, 4491 (2003); 10.1063/1.1606094



Selective particle capture by asynchronously beating cilia

Yang Ding^{1,2,a)} and Eva Kanso^{2,b)}

¹*Beijing Computational Science Research Center, No. 10 Dongbeiwang West Road, Hai-Dian District, Beijing 100094, China*

²*Aerospace and Mechanical Engineering, University of Southern California, Los Angeles, California 90089, USA*

(Received 5 February 2015; accepted 8 December 2015; published online 28 December 2015)

Selective particle filtration is fundamental in many engineering and biological systems. For example, many aquatic microorganisms use filter feeding to capture food particles from the surrounding fluid, using motile cilia. One of the capture strategies is to use the same cilia to generate feeding currents and to intercept particles when the particles are on the downstream side of the cilia. Here, we develop a 3D computational model of ciliary bands interacting with flow suspended particles and calculate particle trajectories for a range of particle sizes. Consistent with experimental observations, we find optimal particle sizes that maximize capture rate. The optimal size depends nonlinearly on cilia spacing and cilia coordination, synchronous vs. asynchronous. These parameters affect the cilia-generated flow field, which in turn affects particle trajectories. The low capture rate of smaller particles is due to the particles' inability to cross the flow streamlines of neighboring cilia. Meanwhile, large particles have difficulty entering the sub-ciliary region once advected downstream, also resulting in low capture rates. The optimal range of particle sizes is enhanced when cilia beat asynchronously. These findings have potentially important implications on the design and use of biomimetic cilia in processes such as particle sorting in microfluidic devices. © 2015 AIP Publishing LLC. [<http://dx.doi.org/10.1063/1.4938558>]

I. INTRODUCTION

The separation and filtration of particles in a fluid medium are essential to many technological and biological processes. Technological applications include controlling indoor and outdoor air quality, manufacturing pharmaceuticals and powders, and sorting cells in microfluidic “lab-on-chip” devices.^{1,2} The health of aquatic ecosystems is largely impacted by filter feeding animals, which provide attractive biological paradigms for particle filtration. Filter feeders remove particulate food from the surrounding water by passing the water over specialized filtering structures. They span multiple length scales and use multifarious feeding structures, from baleen plates to ciliated cells. Borrowing from the aerosol filtration theory, five filter feeding mechanisms have been proposed: sieving, direct interception, inertial impaction, gravitational deposition, and diffusive deposition.^{3,4} These mechanisms often act in combination depending on the flow regime. For example, at high Reynolds number (Re), diffusive deposition is negligible, while the compression of streamlines around the feeding structure provides a potential mechanism for increased encounter of particles.⁵ At low Re , inertia is negligible and the feeding structure has to manipulate the surrounding fluid to generate feeding currents that bring suspended particles closer to the feeding organ.

In this paper, we analyze particle capture by a ciliated model system at low Re . Cilia are slender hair-like structures, typically 5–25 μm in length, that extend from the cell surface. Many microorganisms including marine larvae use motile cilia to generate feeding currents.^{6–8} Cilia-generated flows are characterized by low Re , of the order 10^{-4} to 10^{-2} even in water, where Stokes equations are

^{a)}Electronic mail: dingyang@csr.cac.cn

^{b)}Electronic mail: kanso@usc.edu

applicable. To break the time reversibility inherent in the Stokes regime, motile cilia typically use two mechanisms: (1) an asymmetric beating pattern at the level of the individual cilium, and (2) a metachronal wave pattern in cilia beating collectively. The asymmetric beating pattern consists of an *effective stroke* where the cilium is relatively straight and generates flow in the same direction as its motion and a *recovery stroke* where it bends parallel to the surface and generates a relatively weaker backward flow. The metachronal wave in collectively beating cilia is the result of all cilia performing similar beating patterns, but deforming in time with a small phase difference with respect to their neighbors. Random coordination in beating cilia has also been observed in experiments,^{9,10} however, there is limited understanding of its role in fluid transport. Biofluid mechanics research has focused primarily on analyzing the beating pattern and metachronal coordination in cilia acting individually¹¹ and collectively,^{12–15} with particular emphasis on their role in fluid transport and mixing.

Cilia-driven filter feeders must generate feeding currents and meet the additional challenge of capturing suspended particles. Various capture strategies have been documented in ciliated filter feeders, ranging from ciliary sieving to upstream interception of particles, particle trapping, and downstream particle interception.⁷ Experimental observations suggest that particle capture process by downstream interception is passive and mechanical; that is, it does not seem to rely on active sensing of the suspended particles.¹⁶ Fig. 1 shows the microorganism *Loxosoma pectinaricola* as a representative example. The ciliated organ is characterized by a band of cilia that serves the dual function of generating feeding currents and directly intercepting particles downstream of the cilia.⁷ It is hypothesized that downstream particle collection is based on the “catch-up” principle.¹⁰ According to this principle, cilia move the fluid with suspended particles into the ciliary region, where the same cilia, during their effective stroke, catch up with suspended particles and transfer them to a food groove or mouth cavity. A key point here is that capture takes place during the effective stroke when the “front side” of the cilium catches up with the particle. This qualitative analysis provides valuable insights into the particle capture method but does not elucidate the hydrodynamic mechanisms underlying cilia-particle interactions.

Hydrodynamics plays an important role in particle capture, allowing particles to be transported at higher rates than those associated with diffusion alone. Indeed, considering that the relevant particle size is as small as $1\ \mu\text{m}$, the associated diffusivity at room temperature in water¹⁷ is of the order of $D \sim 10^{-10}$ to $10^{-12}\ \text{m}^2\ \text{s}^{-1}$. Meanwhile, experimental observations of cilia-generated flows report flow speeds of the order $U \sim 100\text{--}1000\ \mu\text{m/s}$,¹⁸ and even as high as $3000\ \mu\text{m/s}$.¹⁹ Thus, estimating conservatively, particles traverse a distance $L \sim 100\ \mu\text{m}$ in approximately $L/U \sim 1\ \text{s}$, whereas particles transported by diffusion alone take a considerably longer time, $L^2/D \sim 100\ \text{s}$. The ratio of diffusive to advective time scales is measured by the Péclet number ($\text{Pe} = UL/D$). For $\text{Pe} \ll 1$, diffusion is dominant. Here, $\text{Pe} \sim 100$ signifying a dominance of advection over diffusion.

In this study, we neglect diffusion and analyze the hydrodynamics of downstream capture in the context of a model system consisting of a band of equally spaced motile cilia (see Fig. 3). Recent numerical studies of particle capture by ciliary fields include continuum envelope models²⁰ that optimize metachronal coordination for feeding and swimming efficiencies as well as discrete particle-cilia

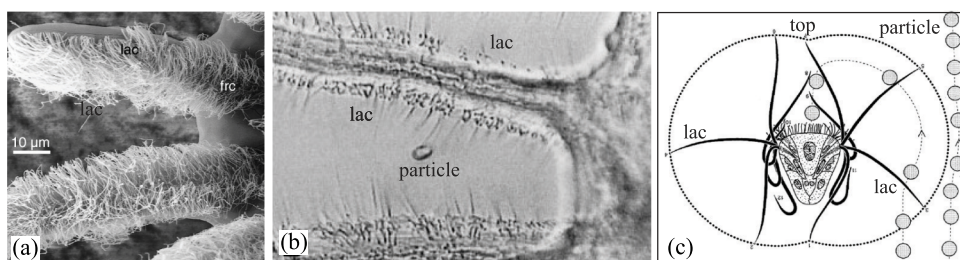


FIG. 1. Particle capture by the cilia on the tentacles of *Loxosoma pectinaricola*. (a) A top view picture of the cilia-covered tentacles. (b) A top view snapshot taken during the particle capture process. (c) A side view illustrative diagram of a particle capture mechanism proposed by Riisgård *et al.*¹⁰ “lac” in the figure represents lateral (compound) cilia. Adapted with permission from H. U. Riisgård, C. Nielsen, and P. S. Larsen, “Downstream collecting in ciliary suspension feeders: The catch-up principle,” *Mar. Ecol.: Prog. Ser.* **207**, 33–51 (2000). Copyright 2000 Inter-Research.

models.^{21–23} The discrete models examine the trapping and transport of a large particle moving above a ciliary carpet,²¹ the capture and release of particles by four cilia beating in synchrony at the corners of a square domain,²² and the downstream capture of particles moving in an “effective” unsteady flow field²³ which does not explicitly account for the beating cilia, and thus exclude cilia spacing and details of particle capture. Here, we account for cilia-particle interactions. We particularly focus on the size spectrum of captured particles and the effect of beating coordination, e.g., synchronous vs. asynchronous, on the size selectivity. From a purely geometric argument, one may expect the size spectrum to be bounded by the cilia spacing and length. Particles need to be smaller than the space between cilia to pass through, and a cilium cannot encircle particles much larger than its length.¹⁰ This thinking proved to be too simplistic. Our results show that the cilia beating coordination affects the particle-size spectrum in a nontrivial manner. These findings have potentially important implications on the design and use of biomimetic cilia in processes such as particle sorting in microfluidic devices. This potential is particularly compelling in light of the rapid development in microscale manufacturing technologies. Indeed, a variety of biomimetic cilia have been demonstrated recently at different scales and using different actuation mechanisms.^{24–27}

II. MODEL

We consider an infinite row of cilia whose base points are placed on a straight line chosen to coincide with the y -axis, where (x, y, z) are properly chosen Cartesian coordinates. The y -distance between the base points of two neighboring cilia is s . The length of each cilium is l . The cilia beat in the xz -plane with frequency ω and period $T = 2\pi/\omega$. We use l and $1/\omega$ to scale length and time, respectively. All variables are thereafter non-dimensional.

The planar beating motion of an individual cilium is represented in a Cartesian frame attached at the base of the cilium by $\xi_c(\sigma, t) \equiv (\xi_x(\sigma, t), 0, \xi_z(\sigma, t))$, where σ is the arclength along the cilium’s centerline from its base ($0 < \sigma < l$) and t is time ($0 < t < T$). We prescribe $\xi_x(\sigma, t)$ and $\xi_z(\sigma, t)$ using Taylor series in σ and Fourier series expansions in t with coefficients based on experimental data,²⁸ see Fig. 2(a). The length of the cilium from these experimental data varies slightly. Here, we rescale the length of the cilium to ensure it is constant, equal to 1, at all times.

For computational convenience, we replace the infinite row of cilia by a finite row of n_c cilia ($n_c \in N$) and impose periodic boundary conditions in the y -direction. For the n th cilium in a periodic domain, the root of the cilium is placed at the point $(0, ns, 0)$ ($n \in \mathbb{Z}$) and its kinematics at time t is

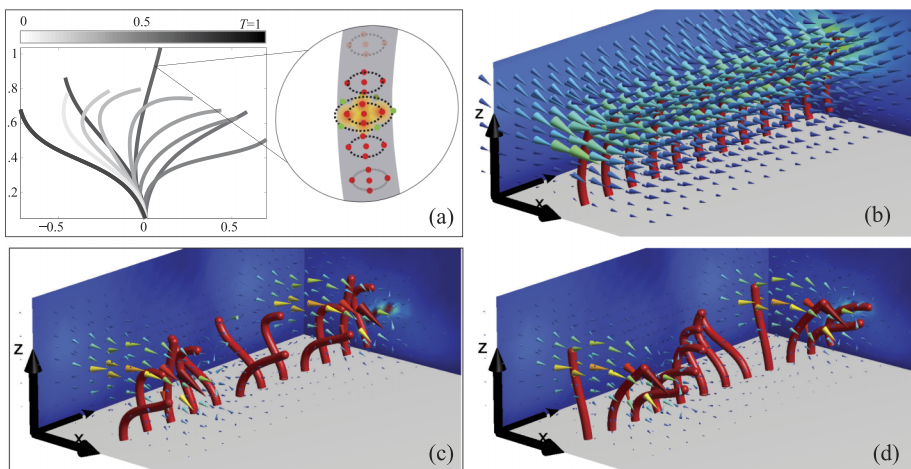


FIG. 2. Cilia kinematics: (a) Beating kinematics of single cilium is taken from the work of Fulford and Blake.²⁸ Color represents time. Inset: Positions of the regularized Stokeslets are indicated by red dots and locations where boundary conditions are enforced that are indicated by green dots. A row of cilia beating (b) in synchrony, (c) at random phase, and (d) in a metachronal wave. The arrows represent the fluid velocity generated by the cilia, and their color indicates the magnitude of the fluid velocity.

given by the position of the centerline,

$$\xi_c(\sigma, t) = (\xi_x(\sigma, t_n), ns, \xi_z(\sigma, t_n)), \quad t_n = \omega t + \phi(n). \quad (1)$$

That is to say, all cilia in the periodic domain undergo the same beating motion but at different phases $\phi(n)$. In particular, we consider three types of phase coordination: (i) cilia beating in synchrony, (ii) cilia beating at random phase differences relative to their neighbors, and (iii) cilia beating in metachrony where each cilium undergoes the same cyclic motion as its neighbor but at a constant phase difference $\phi(n) = 2\pi n/n_c$, see Figs. 2(b)–2(d). In the case of the randomly beating cilia, the phase of a cilium $\phi(n)$ is chosen from a uniform probability distribution function in $(0, 2\pi)$.

The Reynolds number associated with beating cilia is much smaller than 1 and thus, the fluid motion is governed by the Stokes equations and the incompressibility condition

$$-\nabla p + \mu \nabla^2 \mathbf{u} = 0, \quad \nabla \cdot \mathbf{u} = 0, \quad (2)$$

where p is the pressure field, \mathbf{u} is the fluid velocity field, and μ is the dimensionless fluid viscosity. We emphasize that p and \mathbf{u} are functions of position $\mathbf{x} \equiv (x, y, z)$ and time t . The no-slip boundary condition requires the fluid velocity $\mathbf{u}|_{\text{boundary}}$ to be equal to the cilia velocity \mathbf{u}_c at cilia surface and to be identically zero at the wall $z = 0$ together with proper decay at infinity. Here, \mathbf{u}_c is the prescribed velocity of the cilia $\partial \xi_c / \partial t$.

We solve these equations numerically using the method of regularized Stokeslets.²⁹ To compute the flow field generated by the ciliary motion, each cilium is approximated by a distribution of regularized Stokeslets, together with an “image” distribution to satisfy the zero-flow boundary conditions at the wall $z = 0$.³⁰ Expressions for the Green’s function $\mathbf{G}(\mathbf{x}, \mathbf{x}_o)$ corresponding to a regularized Stokeslet at a point \mathbf{x}_o and its image system can be found in the work of Ainley *et al.*³⁰ The strength \mathbf{F} of a regularized Stokeslet depends on its position along the cilium and on time. The total fluid velocity induced by all the Stokeslets is given by

$$\mathbf{u}(\mathbf{x}, t) = \sum_{n=-N_{\max}}^{N_{\max}} \sum_{k=1}^K \mathbf{G}(\mathbf{x}, \mathbf{x}_{n,k}(t)) \cdot \mathbf{F}(\mathbf{x}_{n,k}(t)), \quad (3)$$

where $\mathbf{x}_{n,k}(t)$ is the position of the k th Stokeslet on the cilium identified by n , and $K = 500$ is the total number of Stokeslets per cilium. We approximate the infinitely many copies of cilia due to the periodic boundary conditions by a finite number of copies of the domain equal to $2N_d$, not accounting for the base domain, such that $N_{\max} = n_c(1 + 2N_d)/2$. The regularized Stokeslets $\mathbf{x}_{n,k}$ are commonly placed at the cilium centerline \mathbf{x}^c ,^{14,15} and the regularization parameter is chosen to reflect the finite radius r_c of the cilium.²⁹ While such a discretization properly approximates the far-field flow, it does not produce accurate flow results near the cilia boundaries. A higher precision near the cilia boundaries is needed to study particle capture by the cilia. We thus approximate the cross-sectional area of the cilium using a distribution of five regularized Stokeslets located at a radial position equal to $r_c/2$ from the cilium centerline and the center at each cross section, see the inset of Fig. 2(a). We set the regularization parameter to be $r_c/2$ and we impose the no-slip boundary conditions at 5 points on the surface of the cilium (i.e., at r_c) in each cross section. Boundary conditions applied at those surface points yield that $\mathbf{u}(\mathbf{x}_{n,k}, t) = \partial \xi_c / \partial t$, which, upon substituting (3), yield a linear system of equations. This system is solved numerically using the Generalized Minimum Residual (GMRES) algorithm in MATLAB (MathWorks) to obtain the Stokeslet strengths \mathbf{F} . In turn, the fluid velocity field $\mathbf{u}(\mathbf{x}, t)$ can be reconstructed everywhere using (3).^{14,15,29} This implementation ensures that the average numerical error in the reconstructed velocity at the cilia boundary is less than 5% near the cilia tip and much smaller along the main surface of the cilia. Snapshots of the cilia-generated velocity fields are depicted in Figs. 2(b)–2(d) for cilia beating in synchrony, at random phase, and in metachrony, respectively. Fig. 3 shows the net displacement field of passive tracers over one beating cycle $\mathbf{d}(\mathbf{x}) = \int_0^T \mathbf{u}(\mathbf{x}(t), t) dt$.

We consider the motion of passive spherical particles, of diameter d_p and located at \mathbf{x}_p , in cilia-generated flows. The particles are assumed to move according to $\dot{\mathbf{x}}_p = \mathbf{u}(\mathbf{x}_p, t) + \mathbf{v}$, where \mathbf{v} accounts for steric particle-cilia interactions and is identically zero when a particle is not in direct contact with the cilia. Note that inertial effects are neglected given the small particle size,²³ particle-particle interactions are also neglected. Particles are essentially treated as passive tracers, with velocity equal to the

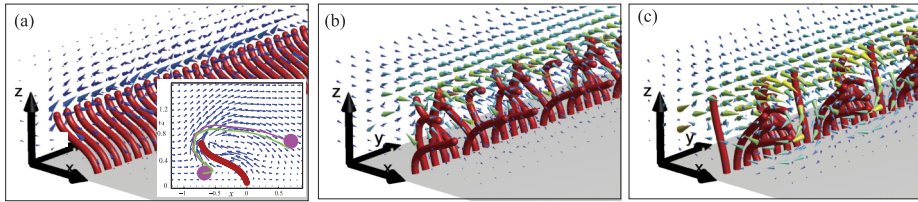


FIG. 3. Displacement field of passive tracers per cycle for (a) synchronously beating cilia; inset shows the y -averaged displacement field; (b) cilia beating at random phase; and (c) cilia beating in a metachronal wave. For clarity, the displacements in (b) and (c) are scaled by 0.5. In the inset, the green and magenta lines represent the trajectories of two particles with $d_p = 0$ and $d_p = 0.20$, respectively.

fluid velocity at the particle center. This is consistent with recent findings on a similar configuration which show that even for the particle sizes comparable to cilia movement, the difference between the motion of the fully resolved particles and that of passive tracers is small.³¹

When the particles get in contact with cilia, based on recent observations that particles are captured by cilia moving in the flow direction,^{10,32} we distinguish between two events: if a given particle is touched by the “front side” of the cilia, it gets captured. In biological systems, complex particle-organism interactions occur after downstream interception and the particle gets eventually removed from the capture region either directly or by other cilia and/or mouth-induced flows.^{10,32} If, on the other hand, a particle gets in contact with the “back side” of the cilia, a repulsive velocity normal to the surface of the cilium is added to ensure collision avoidance, i.e., that the particle does not penetrate the cilium and at the same time and does not get captured on the “back side” of the cilia. These modeling assumptions are consistent with experimental observation of particle capture by downstream interception¹⁰ and the fact that cilia bend into the flow direction and are thus able to intercept particles during their effective but not recovery stroke. However, without further experimental data in the literature to support a particular model for the near-field interactions between the particle and neighboring cilia, we simply let $\mathbf{v} = (\mu\Delta)\mathbf{n}$, where μ is a large constant coefficient, Δ is the overlap between the cilium and the particle, and \mathbf{n} is the local normal to the cilium. This model of particle-cilia interaction is illustrated in Fig. 4(a). This steric particle-cilia interaction affects the particle trajectories in a non-trivial manner as depicted in the inset of Fig. 3(a), which highlights the difference between the motion of a passive tracer (green) and a particle of size $d_p = 0.20$ (magenta). The deviation between the two trajectories is due to the steric interactions with the cilia.

III. RESULTS

We examine the cilia’s ability to capture flowborne particles. We consider particles that are initially placed in a volume on a regular 3D uniform grid with grid size equal to 0.1 unit length. The number of particles per unit volume is $n_p = 1000$. The particles are placed upstream of the cilia so that the fresh fluid that can be filtered by the cilia is entirely seeded with particles, see Fig. 4(a).

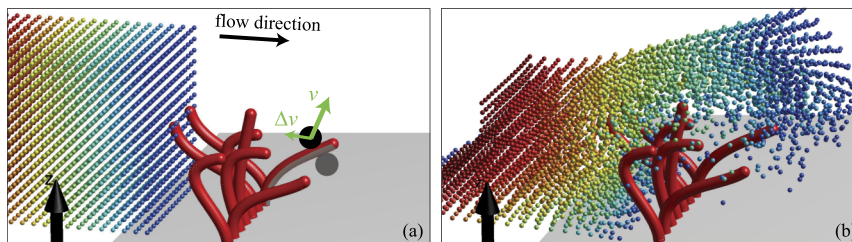


FIG. 4. Particle motion in cilia-generated flows: (a) initial particle seeding; (b) particle distribution after 7 cycles. The parameter values are $s = 0.2$ and $d_p = 0.04$. The black and gray particles in (a) illustrate the cilia-particle interaction model: the black particle in contact with the back side of a cilium gets pushed away due to an additional velocity \mathbf{v} , while the gray particle in contact with the front side of the cilium (gray area) is captured by the cilium.

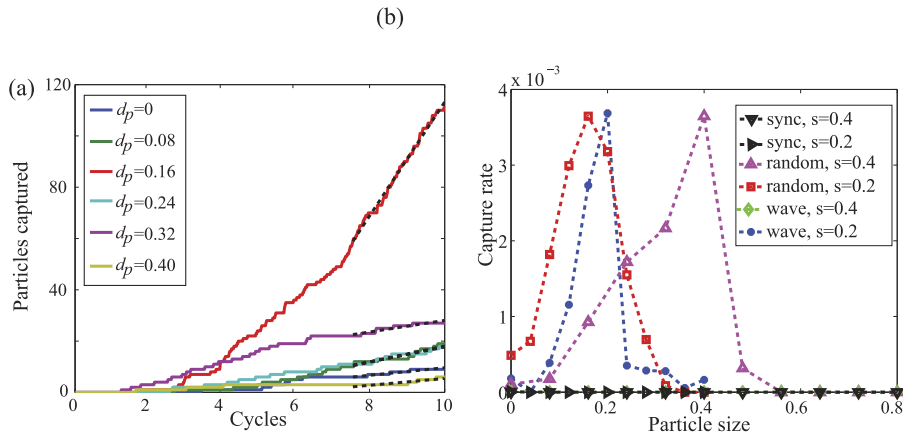


FIG. 5. Particle capture by cilia array: (a) the number of particles captured as a function of time. The dashed lines correspond to the best linear fit after the 7th cycle. Colors represent different particle sizes; (b) capture rate as a function of particle size d_p and separation distance between cilia s .

Cilia-generated flows drive the particles towards the cilia, see Fig. 4(b), where they are either captured or deflected away from the cilia depending on their position relative to the cilia. We emphasize that the trajectory of each particle is calculated independently (no particle-particle interaction). Fig. 5(a) shows that the number of cilia-captured particles is zero for the first few cycles and increases almost linearly with time thereafter. We neglect the initial transience and use a linear fit to obtain the number of particles captured per unit cycle, which we denote by k , see Fig. 5(a). We then define the *capture rate* $\eta = k/n_p/n_c$ as the number of particles captured per cycle normalized by the total number of particles per unit volume n_p and by the total number of cilia n_c in the periodic domain. That is to say, the units of η are the number of particles captured per cycle per cilium per number of particles in unit volume.

No particles are captured when the cilia beat in synchrony, see Fig. 5(b). This result is independent of particle size d_p and the separation distance s between neighboring cilia. It is mostly due to the nearly 2D nature of the cilia-generated flows in the case of synchronously beating cilia, because of the 2D ciliary beating pattern employed here (Fig. 2(a)). Indeed, the associated displacement field of passive tracers, see the inset in Fig. 3(a), shows that particles would encounter the front side of the cilia where capture occurs only if they enter the small recirculation region downstream of the cilia. However, upstream particles first touch the back side of the cilia and, thus, get pushed further away, making it impossible for them to reach the downstream recirculation region and get captured.

When the cilia beat at random phase or in metachronal wave, the capture rate η is sensitive to both the particle size d_p and the separation distance s between neighboring cilia. Capture rate is zero for the metachronal wave with $s = 0.4$. For other three cases, Fig. 5(b) shows that η increases and then decreases with particle size indicating the presence of an optimal particle size that maximizes capture. Both the optimal particle size and the capture rate depend on the type of coordination (random or metachronal) and the spacing s between neighboring cilia. For the smaller spacing $s = 0.2$, the capture rate is comparable for the cilia beating in metachronal wave and for the cilia beating at random phase. However, for larger spacing $s = 0.4$, the cilia with random phase capture more particles and the maximal capture rate occurs at larger particle size. Particles larger than the spacing s can be captured but the capture rate decreases with increasing particle size.

Finally, we examine the position and timing (or phase) of particle capture. We find that capture occurs mostly in the first half of the effective forward stroke as indicated in Figs. 6(a) and 6(d). We also recorded the location along the cilium where capture is most likely to occur. Fig. 6(c) shows that the part close to the tip of the cilia captured more particles in the case of metachronal beating. In the random phase case, the top half of the cilia still captured more particles but the captured particles are more evenly distributed along the whole length of the cilia.

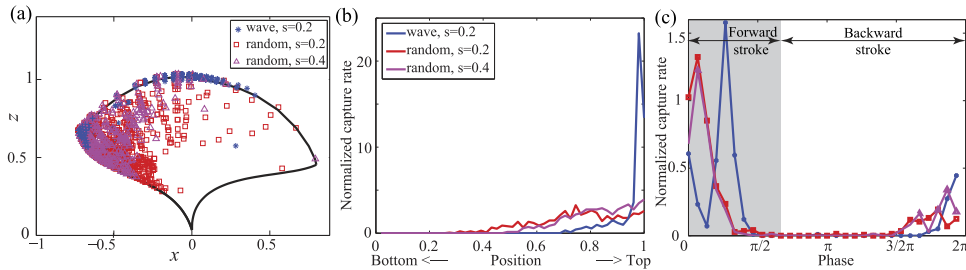


FIG. 6. Spatial and temporal distributions of the capture events: (a) positions of captured particles projected onto the (x, z) -plane. Black lines represent the outline of the region swept by a beating cilium during its effective and recovery stroke; (b) location along the cilia where the particles get captured. Capture rate is normalized so that the area under each line is 1; (c) phase at which capture occurs. Gray region indicates the phase corresponding to forward effective stroke.

IV. DISCUSSION

We proposed a discrete model system for particle capture by bands of synchronously and asynchronously beating cilia. The model is motivated by the “catch-up” mechanism for downstream particle capture. The hydrodynamic picture revealed by our model is more complicated than previously proposed. Previous studies have hypothesized that downstream capture occurs when cilia move faster during the forward stroke compared to suspended particles. Our results show that instantaneously faster movement of cilia during the forward stroke is neither sufficient nor necessary for particle capture. For instance, synchronously beating cilia do not capture suspended particles even though their speed exceeds that of the suspended particles during the effective stroke. Asynchronously beating cilia, whether metachronally or randomly, selectively capture particles from a size spectrum ranging between 0.1 and 0.4 length units (see Fig. 5(b)), which translate to particles between 2 and 5 μm in diameter for typical cilia length of 20 μm . These results are consistent with experimental observations of particle capture by ciliated microorganisms¹⁰ (Fig. 17). Note that Fig. 5(b) reports capture rate as defined in Sec. III, whereas Riisgård and co-authors¹⁰ measure particle retention in percentage form.

We also probed the model to reveal the effects of cilia spacing and cilia coordination on particle capture. Our results show that the particle-size spectrum is sensitive to both cilia spacing and cilia coordination. For metachronally beating cilia, decreasing cilia spacing enables particle capture, while decreasing cilia spacing in randomly beating cilia affects both lower and upper size limits (see Fig. 5(b)). This nonlinear dependence of particle size spectrum on cilia parameters is a clear indication of the role of hydrodynamics in coupling cilia coordination to particle capture rate. The hydrodynamic picture we obtained suggests that small particles have difficulty moving across streamlines near the surface of the cilia, while large particles have difficulty entering the sub-ciliary region after passing the cilia tips. The metachronal or random beating of cilia helps in manipulating the flow field near the cilia in a way that could be exploited to enhance the particular capture rate.

We conclude by noting that our aim here was to highlight the fluid mechanics effects on particle capture by ciliary bands and we thus neglected effects such as the particle Brownian motion and particle-particle interactions. The latter will be incorporated in future extensions of the current model.

ACKNOWLEDGMENTS

We thank the Center for High-Performance Computing and Communications at USC for providing HPC resources and support. E.K. and Y.D. are indebted to Dr. Janna Nawroth and Professor Margaret McFall-Ngai for many useful discussions. Y.D. thanks Longhua Zhao for useful discussion.

¹ V. Lecault, A. K. White, A. Singhal, and C. L. Hansen, “Microfluidic single cell analysis: From promise to practice,” *Curr. Opin. Chem. Biol.* **16**, 381–390 (2012).

² E. L. Jackson and H. Lu, “Advances in microfluidic cell separation and manipulation,” *Curr. Opin. Chem. Eng.* **2**, 398–404 (2013).

³ D. I. Rubenstein and M. Koehl, “The mechanisms of filter feeding: Some theoretical considerations,” *Am. Nat.* **111**, 981–994 (1977).

- ⁴ M. LaBarbera, "Feeding currents and particle capture mechanisms in suspension feeding animals," *Am. Zool.* **24**, 71–84 (1984).
- ⁵ S. Humphries, "Filter feeders and plankton increase particle encounter rates through flow regime control," *Proc. Natl. Acad. Sci. U. S. A.* **106**, 7882–7887 (2009).
- ⁶ J. Shimeta and M. Koehl, "Mechanisms of particle selection by tentaculate suspension feeders during encounter, retention, and handling," *J. Exp. Mar. Biol. Ecol.* **209**, 47–73 (1997).
- ⁷ H. U. Riisgård and P. S. Larsen, "Minireview: Ciliary filter feeding and bio-fluid mechanics—Present understanding and unsolved problems," *Limnol. Oceanogr.* **46**, 882–891 (2001).
- ⁸ T. Fenchel, "Suspension feeding in ciliated protozoa: Functional response and particle size selection," *Microb. Ecol.* **6**, 1–11 (1980).
- ⁹ J. Nawroth and J. Dabiri, "Hydrodynamic interactions of bacteria and particles with ciliated surfaces," *Bull. Am. Phys. Soc.* **59**, Abstract ID: BAPS.2014.DFD.A9.5 (2014).
- ¹⁰ H. U. Riisgård, C. Nielsen, and P. S. Larsen, "Downstream collecting in ciliary suspension feeders: The catch-up principle," *Mar. Ecol.: Prog. Ser.* **207**, 33–51 (2000).
- ¹¹ C. Eloy and E. Lauga, "Kinematics of the most efficient cilium," *Phys. Rev. Lett.* **109**, 038101 (2012).
- ¹² S. Michelin and E. Lauga, "Efficiency optimization and symmetry-breaking in a model of ciliary locomotion," *Phys. Fluids* **22**, 111901 (2010).
- ¹³ N. Osterman and A. Vilfan, "Finding the ciliary beating pattern with optimal efficiency," *Proc. Natl. Acad. Sci. U. S. A.* **108**, 15727–15732 (2011).
- ¹⁴ H. Guo, J. Nawroth, Y. Ding, and E. Kanso, "Cilia beating patterns are not hydrodynamically optimal," *Phys. Fluids* **26**, 091901 (2014).
- ¹⁵ Y. Ding, J. C. Nawroth, M. J. McFall-Ngai, and E. Kanso, "Mixing and transport by ciliary carpets: A numerical study," *J. Fluid Mech.* **743**, 124–140 (2014).
- ¹⁶ C. M. Boyd, "Selection of particle sizes by filter-feeding copepods: A plea for reason," *Limnol. Oceanogr.* **21**, 175–180 (1976).
- ¹⁷ A. Einstein, "On the theory of the Brownian movement," *Ann. Phys.* **4**, 371–381 (1906).
- ¹⁸ O. H. Shapiro, V. I. Fernandez, M. Garren, J. S. Guasto, F. P. Debaillon-Vesque, E. Kramarsky-Winter, A. Vardi, and R. Stocker, "Vortical ciliary flows actively enhance mass transport in reef corals," *Proc. Natl. Acad. Sci. U. S. A.* **111**, 13391–13396 (2014).
- ¹⁹ R. B. Emlet, "Flow fields around ciliated larvae: Effects of natural and artificial tethers," *Mar. Ecol.: Prog. Ser.* **63**, 211–225 (1990).
- ²⁰ S. Michelin and E. Lauga, "Optimal feeding is optimal swimming for all Péclet numbers," *Phys. Fluids* **23**, 101901 (2011).
- ²¹ A. Bhattacharya, G. A. Buxton, O. B. Usta, and A. C. Balazs, "Propulsion and trapping of microparticles by active cilia arrays," *Langmuir* **28**, 3217–3226 (2012).
- ²² R. Ghosh, G. A. Buxton, O. B. Usta, A. C. Balazs, and A. Alexeev, "Designing oscillating cilia that capture or release microscopic particles," *Langmuir* **26**, 2963–2968 (2009).
- ²³ S. Mayer, "Modelling of ciliary downstream collecting in suspension-feeding invertebrates," *Math. Methods Appl. Sci.* **24**, 1409–1427 (2001).
- ²⁴ A. R. Shields, B. L. Fiser, B. A. Evans, M. R. Falvo, S. Washburn, and R. Superfine, "Biomimetic cilia arrays generate simultaneous pumping and mixing regimes," *Proc. Natl. Acad. Sci. U. S. A.* **107**, 15670–15675 (2010).
- ²⁵ K. Oh, J.-H. Chung, S. Devasia, and J. J. Riley, "Bio-mimetic silicone cilia for microfluidic manipulation," *Lab Chip* **9**, 1561–1566 (2009).
- ²⁶ J. den Toonder, F. Bos, D. Broer, L. Filippini, M. Gillies, J. de Goede, T. Mol, M. Reijme, W. Talen, H. Wilderbeek, V. Khataavkarb, and P. Andersonb, "Artificial cilia for active micro-fluidic mixing," *Lab Chip* **8**, 533–541 (2008).
- ²⁷ M. Vilfan, A. Potočnik, B. Kavčič, N. Osterman, I. Poberaj, A. Vilfan, and D. Babič, "Self-assembled artificial cilia," *Proc. Natl. Acad. Sci. U. S. A.* **107**, 1844–1847 (2010).
- ²⁸ G. R. Fulford and J. R. Blake, "Muco-ciliary transport in the lung," *J. Theor. Biol.* **121**, 381–402 (1986).
- ²⁹ R. Cortez, "The method of regularized Stokeslets," *SIAM J. Sci. Comput.* **23**, 1204–1225 (2001).
- ³⁰ J. Ainley, S. Durkin, R. Embid, P. Boindala, and R. Cortez, "The method of images for regularized Stokeslets," *J. Comput. Phys.* **227**, 4600–4616 (2008).
- ³¹ A. L. Buchmann, L. J. Fauci, K. Leiderman, E. M. Strawbridge, and L. Zhao, "Flow induced by bacterial carpets and transport of microscale loads," in *Applications of Dynamical Systems in Biology and Medicine*, The IMA Volumes in Mathematics and Its Applications (Springer Science & Business Media, 2015), Vol. 158, pp. 35–53.
- ³² M. R. Romero, H. C. Kelstrup, and R. R. Strathmann, "Capture of particles by direct interception by cilia during feeding of a gastropod veliger," *Biol. Bull.* **218**, 145–159 (2010). Pub Med Index, PMID: 20413791.